

## Seismic behavior of steel reinforced concrete special-shaped column-beam joints

Z.Q. Liu\*, J.Y. Xue and H.T. Zhao

*College of Civil Engineering, Xi'an University of Architecture and Technology, Xi'an, China*

*(Received December 31, 2015, Revised September 30, 2016, Accepted October 5, 2016)*

**Abstract.** This paper focuses on the study of seismic behavior of steel reinforced concrete special-shaped column-beam joints. Six specimens, which are designed according to the principle of strong-member and weak-joint core, are tested under low cyclic reversed load. Key parameters include the steel form in column section and the ratio of column limb height to thickness. The failure mode, load-displacement curves, ductility, stiffness degradations, energy dissipation capacity and shear deformation of joint core of the test subassemblies are analyzed. The results indicate that SRC special-shaped column-beam joints have good seismic behavior. All specimens failed due to the shear failure of the joint core, and the failure degree between the two sides of joint core is similar for the exterior joint but different for the corner joint. Compared to the joints with channel steel truss, the joints with solid web steel skeleton illustrate better ductility and energy dissipation capacity, but the loading capacity and stiffness are roughly close. With the increasing of the ratio of column limb height to thickness, the joints illustrate higher loading capacity and stiffness, better energy dissipation capacity, but worse ductility.

**Keywords:** steel reinforced concrete (SRC); special-shaped column; seismic behavior; experimental study; joint core

---

### 1. Introduction

Special-shaped column structure, in which the columns with L-shaped, T-shaped and crisscross-shaped sections are substituted for the conventional rectangular columns, is a new type of structural system (Fig.1). Because of the equal width between column limbs and infilled walls, it has the advantage of saving indoor space and convenient arrangement for furniture. Therefore, the special-shaped column structures are widely employed in the practical engineering. In past decades, the reinforced concrete (RC) special-shaped column structures have been extensively studied. The mechanical behavior and seismic performance of columns, joints and frames were revealed (Dundar and Sahin 1993; Sinha 1996; Balaji and Murty 2001; Cao et al 2002a; Rong et al. 2013; Xiao et al. 2011a). By analyzing the study results, it can be seen that for the RC special-shaped column structures, low bearing capacity and poor ductility are critical issues (Zhou et al. 2012a; Xue et al. 2012b; Tu et al. 2014). In recent years, steel reinforced concrete (SRC) structure

---

\*Corresponding author, Ph.D., E-mail: [liuzuqiang@xauat.edu.cn](mailto:liuzuqiang@xauat.edu.cn)

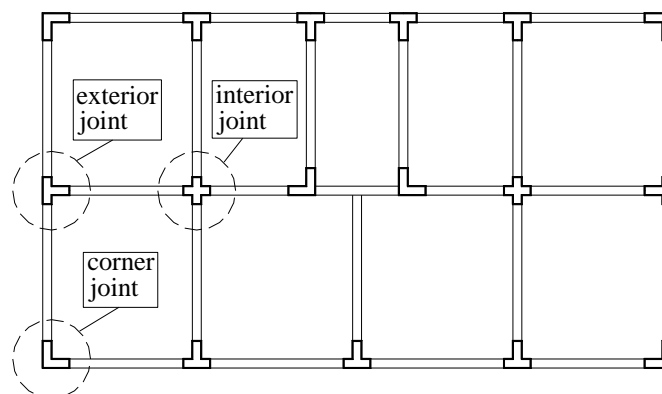


Fig. 1 Plan of special-shaped column structure

has attracted much attention because of their high earthquake resistance (Kim *et al.* 2012c, Chen *et al.* 2009, Ellobody and Yong 2011b). Combining special-shaped column structure and SRC structure, Chen *et al.* (2006) proposed SRC special-shaped column structure.

SRC special-shaped column is the concrete column with special-shaped section, in which the steel as well as longitudinal reinforcement and stirrups are configured. It not only keeps the advantage of special-shaped column structure, but also has the good performance of SRC structure.

Several researches have been conducted to investigate the behaviors of SRC special-shaped column. Tokgoz and Dundar (2012d) examined eight L-shaped columns under biaxially compressive axial load and a theoretical method based on the nonlinear behavior of the material was put forward to describe the L-shaped column behavior. Xue *et al.* (2012b) carried out tests on nine T-shaped columns, four L-shaped columns and four crisscross-shaped columns under low cyclic reversed load, and design formulas for ultimate shear strength of SRC special-shaped column were proposed. Although there are some investigations reported on the behavior of SRC special-shaped columns, the behavior of SRC special-shaped column-beam joint is less studied.

In this paper, low-cyclic reversed loading tests of six SRC special-shaped column-beam joint specimens including three exterior joint (SRC T-shaped column-beam joint) specimens and three corner joint (SRC L-shaped column-beam joint) specimens are carried out to investigate seismic behavior of the joint. The failure mode, load-displacement curves, ductility, stiffness degradations, energy dissipation capacity and shear deformation of the joint core are discussed in detail, and the influence of the steel form in column section and the ratio of column limb height to thickness on the seismic behavior of the joints is concentrated on.

## 2. Experimental program

### 2.1. Specimen design

Exterior joint and corner joint (designated as TJ and LJ, respectively) were selected for the scale model tests. In considerations of the available maximum loading capacity of the actuator and the conditions of the laboratory, the scale ratio of the specimens was determined as 1:2. The details

of the specimens are illustrated in Figs. 2 and 3, and are summarized in Table 1. TJ and LJ each had three specimens with two variable parameters including the steel form in column section and the ratio of column limb height to thickness. Two types of steel forms in column section are configured, including the channel steel truss (for the specimens TJ1, TJ3, LJ1 and LJ3) (Fig. 4(a)), and the solid web steel skeleton (for the specimens TJ2 and LJ2) (Fig. 4(b)). Two kinds of ratios of column limb height to thickness, such as 2 (for the specimens TJ1, TJ2, LJ1 and LJ2) and 3 (for the specimens TJ3 and LJ3), were considered to study the seismic behavior of specimens. Assuming that the positions of the zero-moment inflection points were located at the mid-span of beams and mid-height of columns, the subassemblies along with boundary and loading conditions could simulate part of a frame subjected to an earthquake-induced moment. To facilitate the analysis of the behavior and shear strength of the column-beam joints, the specimens were designed in such a way that the joints are likely to fail first.

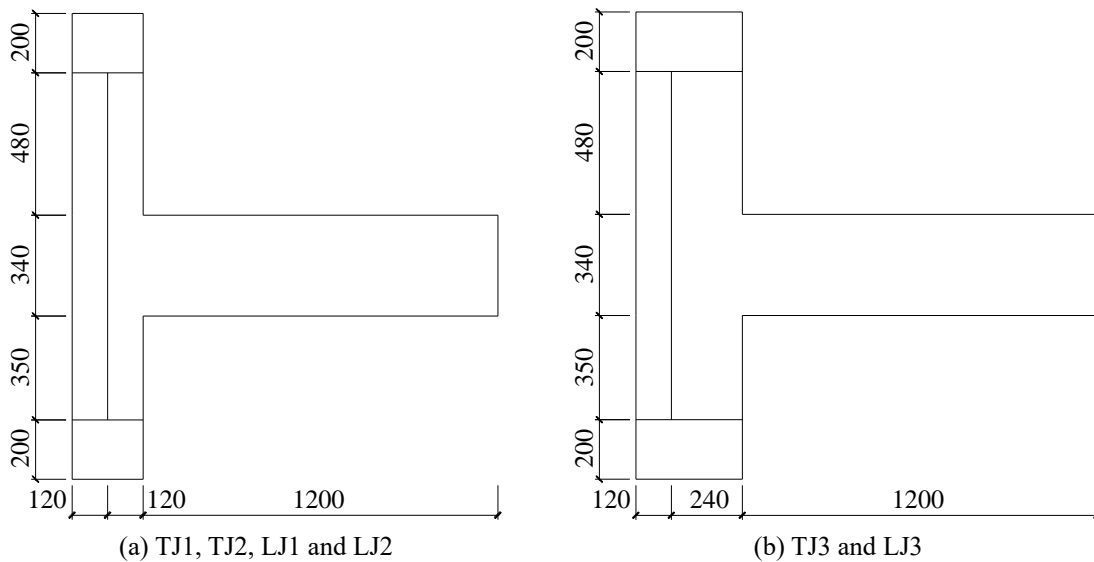


Fig. 2 Geometry and dimensions of the specimens (units: mm)

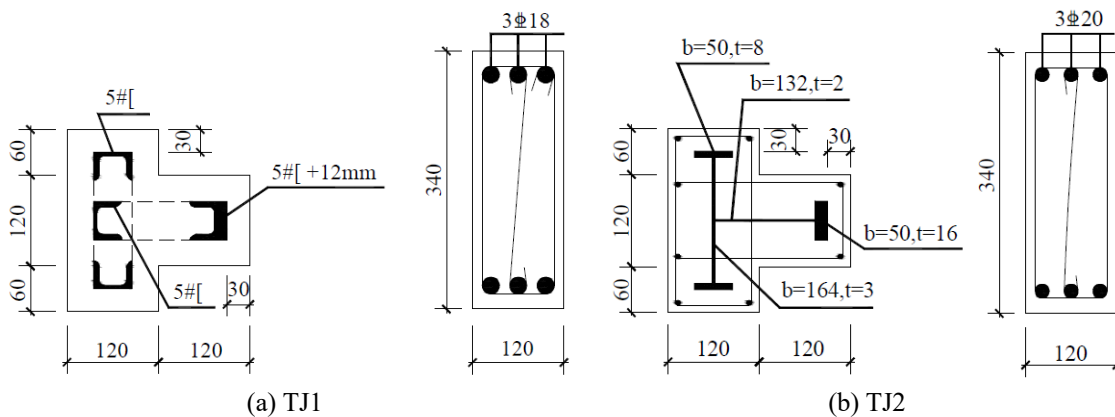


Fig. 3 Sections of columns and beams (units: mm)

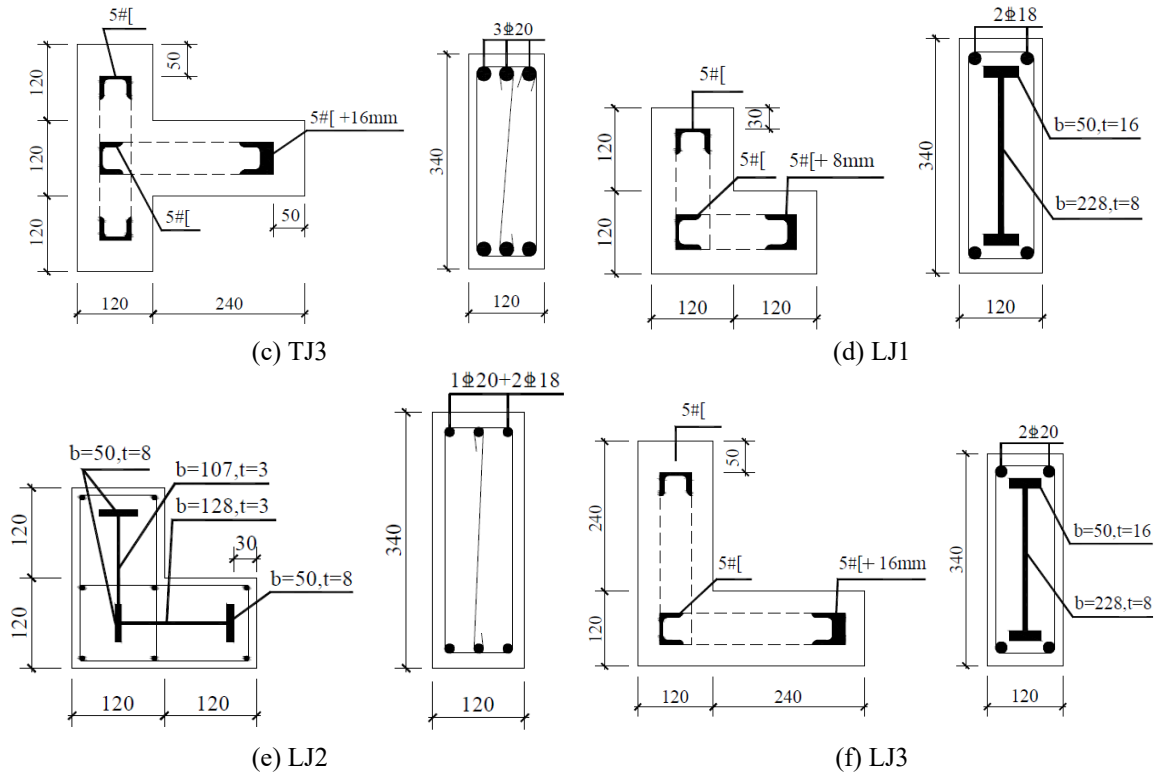


Fig. 3 Continued

## 2.2. Fabrication and material properties

The channel steel truss was manufactured through that the channel steels were connected by using horizontal web members in the form of welding. The configurations of horizontal web members in the joint core are shown in Table 1.  $\phi 8$  bars were used as horizontal web members in

Table 1 Details of the specimens

Specimen	Joint type	Column		Joint core		Beam type
		Steel form	$H/B$	$C_{sw}$ (or $t$ )	$C_{sv}$	
TJ1	Exterior joint	Channel steel truss	2.0	$2\phi 6@94\text{mm}$	-	RC
TJ2	Exterior joint	Solid web steel skeleton	2.0	2mm	$2\phi 4@100\text{mm}$	RC
TJ3	Exterior joint	Channel steel truss	3.0	$2\phi 6@140\text{mm}$	-	RC
LJ1	Corner joint	Channel steel truss	2.0	$2\phi 12@75\text{mm}$	-	SRC
LJ2	Corner joint	Solid web steel skeleton	2.0	3mm	$2\phi 4@100\text{mm}$	RC
LJ3	Corner joint	Channel steel truss	3.0	$2\phi 12@75\text{mm}$	-	SRC

Note:  $H/B$  - Ratio of column limb height to thickness;  $C_{sw}$  - Configuration of horizontal web member;  $t$  - Thickness of steel plate;  $C_{sv}$  - Configuration of stirrup

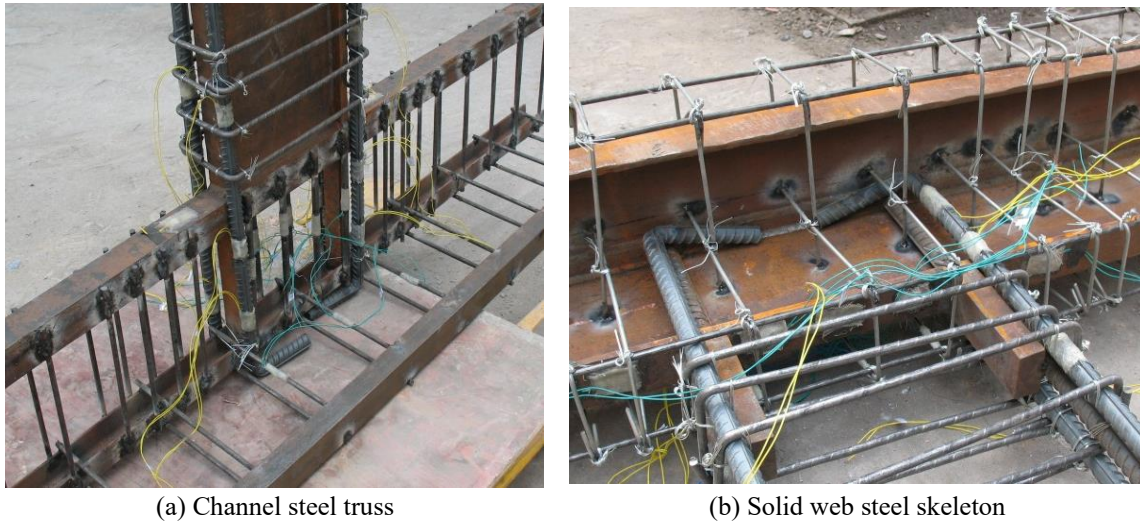


Fig. 4 Steel form

the column, the interval of which was 50 mm at intensive area and 100 mm at non-intensive area. There was no longitudinal steel reinforcement and stirrup in the column with channel steel truss.

The solid web steel skeleton was manufactured through that the steel plates were welded into integral steel with definite shape firstly; and then the stirrups were formed to the U-shaped or the closed rectangular-shaped and welded on the integral steel; finally, the longitudinal steel reinforcements were assembled with the stirrups.  $\phi 6$  bars were used as longitudinal steel reinforcements and  $\phi 4$  bars were used as stirrups with the interval of 50 mm at intensive area and 100 mm at non-intensive area in the column. The configurations of stirrups in the joint core are shown in Table 1.

Table 2 Mechanical properties of steel bars and plates

Material	$D$ or $t$	$f_y$ (MPa)	$f_u$ (MPa)	$E_s$ (MPa)
Steel bars	$\phi 4$	425	444	$1.965 \times 10^5$
	$\phi 6$	551	674	$1.944 \times 10^5$
	$\phi 8$	441	543	$1.921 \times 10^5$
	$\phi 12$	295	440	$1.970 \times 10^5$
	$\phi 18$	453	501	$2.010 \times 10^5$
	$\phi 20$	432	487	$2.050 \times 10^5$
Steel plates	2 mm	236	278	$1.734 \times 10^5$
	3 mm	295	385	$1.950 \times 10^5$
	8 mm	363	503	$1.946 \times 10^5$
	16 mm	320	365	$1.980 \times 10^5$

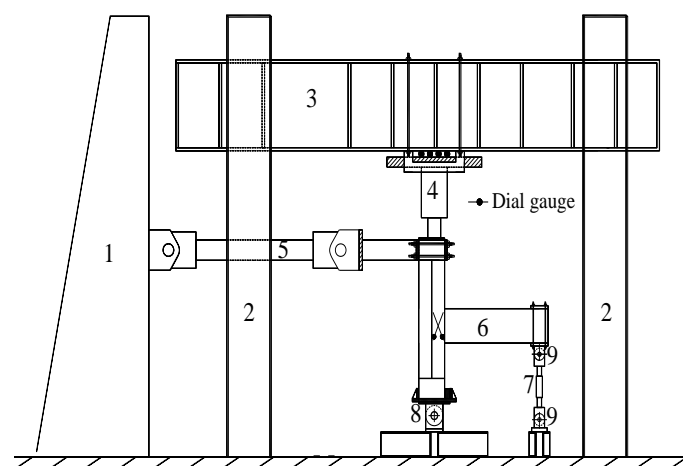
Note:  $D$  - Diameter of steel bar;  $t$  - Thickness of steel plate;  $f_y$  - Yield strength;  $f_u$  - Ultimate strength;  $E_s$  - Elastic modulus

The stirrups of all beams were configured by using  $\phi 8$  bars with the interval of 50 mm at intensive area and 100 mm at non-intensive area. The mechanical properties of the steel bars and plates are given in Table 2. Fine aggregate commercial concrete was used to pour the specimens. The average cubic compressive strength of the concrete (the side length of the standard cubic specimens equals 150 mm) measured at the 28th day was 43.7 MPa.

### 2.3 Test setup and procedure

As shown in Fig. 5, the specimens were pinned at the bottom end of column and beam end and free at the top end of column. The axial compression load was applied to the column through a vertical jack and kept invariable during the test process, and then low cyclic reversed load was applied to the top end of column by the horizontal actuator. Horizontal load was applied using the force-control scheme repeated only once at each control point before the specimen yields and using the displacement-control scheme repeated three times at each control point after the specimen yields, as shown in Fig. 6, in which  $\Delta_y$  denoted the yield displacement. The procedure was continued until the reaction force descended to about 85% of the maximum value. The out-of-plane displacements of the specimens were completely restricted.

The vertical actuator had a 1500 kN capacity in compression, and the horizontal actuator had a force capacity of  $\pm 1000$  kN and a displacement capacity of  $\pm 350$  mm. The instrumentations used in the test were the load cells, linear variable displacement transducer, dial gauges, and strain gauges. The load and displacement of the top end of column were measured respectively by load cell and displacement transducer, which were installed in the horizontal actuator. The load of beam end was measured by load cell. Measurement of the relative rotation at the joint core was given with particular attention. Two dial gauges were set diagonally on the joint core to measure the shear deformation, as shown in Fig. 5. Strain gauges were mounted at the steels, longitudinal steel reinforcement and stirrups to capture strain history of the joint core, column and beam, as shown in Fig. 7.



1.Reaction wall 2.Reaction column 3.Reaction beam 4.Vertical actuator 5.Horizontal actuator  
6.Specimen 7.Load cell 8.Single-hinge support under column 9.Single-hinge support at beam end

Fig. 5 Test setup

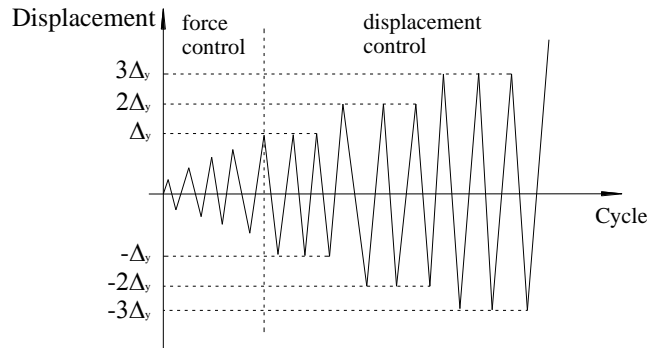


Fig. 6 Loading control process

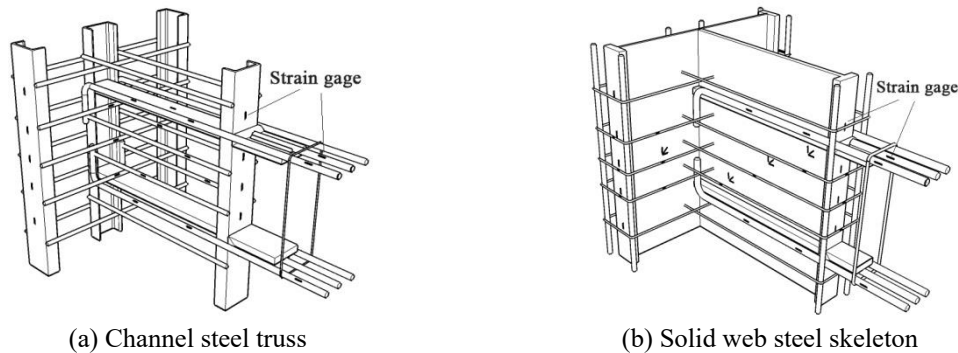


Fig. 7 Positions of strain gages

### 3. Experimental results

#### 3.1 General behavior

The failure mode of all specimens is the shear failure of the joint core, as illustrated in Fig. 8. Since the specimens demonstrated similar phenomenon in the tests, only the specimen TJ2 is discussed here.

At the beginning of the force-control loading stage, flexural cracks occurred at the beam end near the column-beam surface. But with the increasing of force, no evident crack development at the beam end could be observed. When the lateral force reached positive 50 kN, large amounts of diagonal cracks appeared at the joint core and the stirrup and solid web steel of the joint core yielded, as shown in Fig. 9. Then the opposite loading to negative 50 kN resulted in densely distributed crossed diagonal cracks at the joint core and the yielding of the specimen indicated by the load-displacement curve. In the displacement-control loading stage, when the applied displacement firstly reached positive 23 mm, the concrete at the joint core began to crush. After that, the area of the crushing concrete expanded gradually with the increasing of the displacement amplitude. Finally, the shear failure of the joint core could be observed when the positive and negative applied displacement respectively reached 64 mm. At this moment, only a few cracks appeared at the beam and column ends.

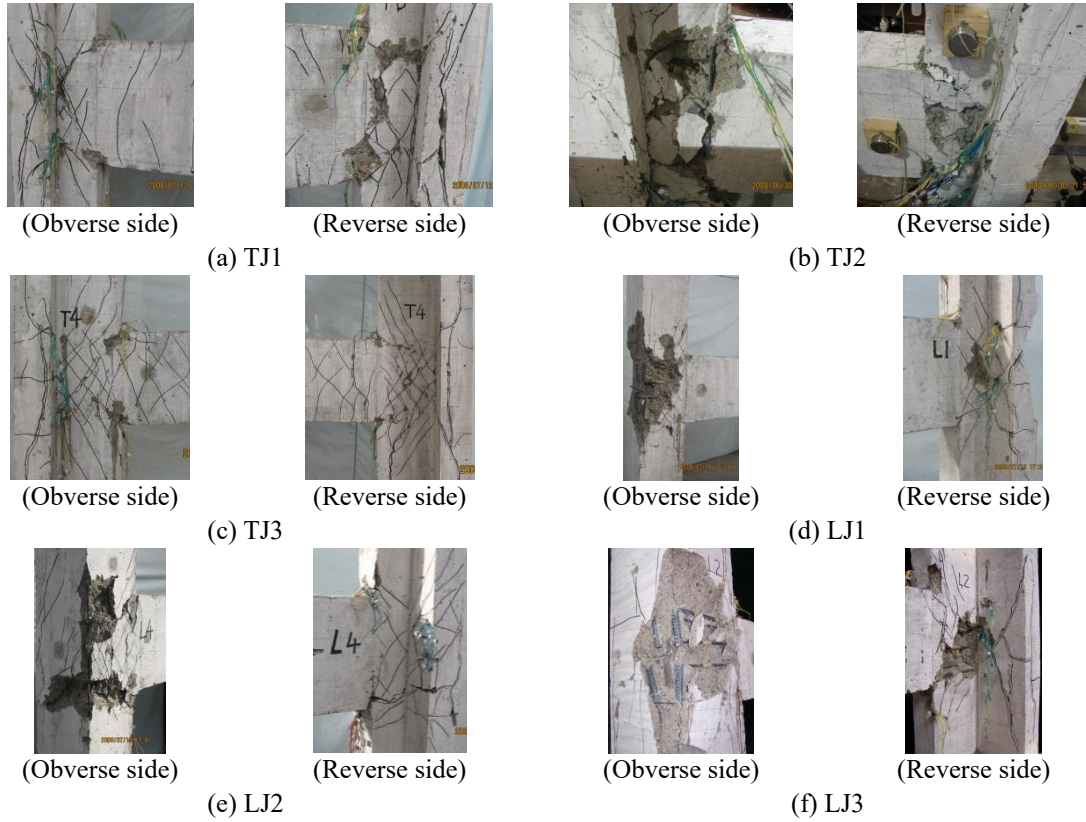


Fig. 8 Failure modes of the specimens

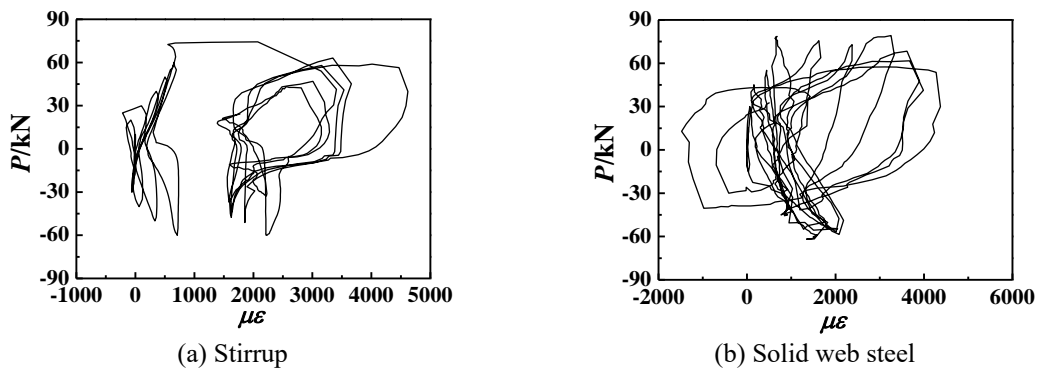


Fig. 9 Strains of steels at the joint core of TJ2

It can be seen from Fig. 8 that for the joint core of exterior joints (TJ), the failure degree between the obverse side and the reverse side is similar, but for the joint core of corner joints (LJ), the failure degree of the reverse side is more serious than that of the obverse side. This is because for the exterior joint, the action line of horizontal load passes the figure center and the flexural center of T-shaped section simultaneously, and there is only shear force at the joint core section.

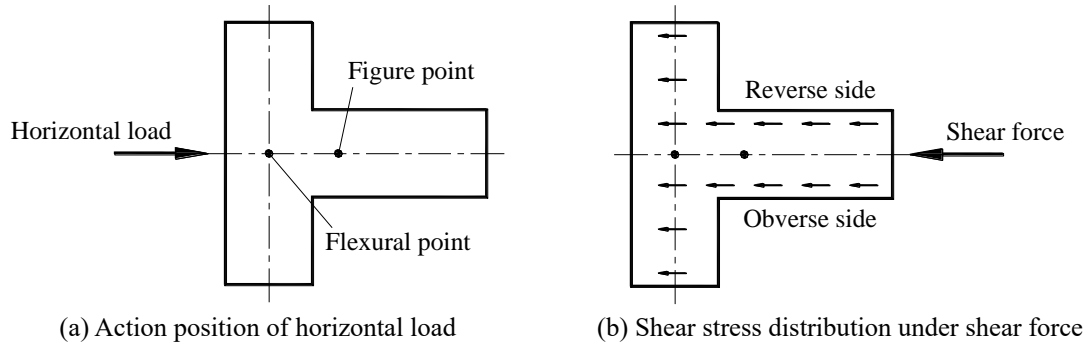


Fig. 10 Mechanical state of the joint core of exterior joint

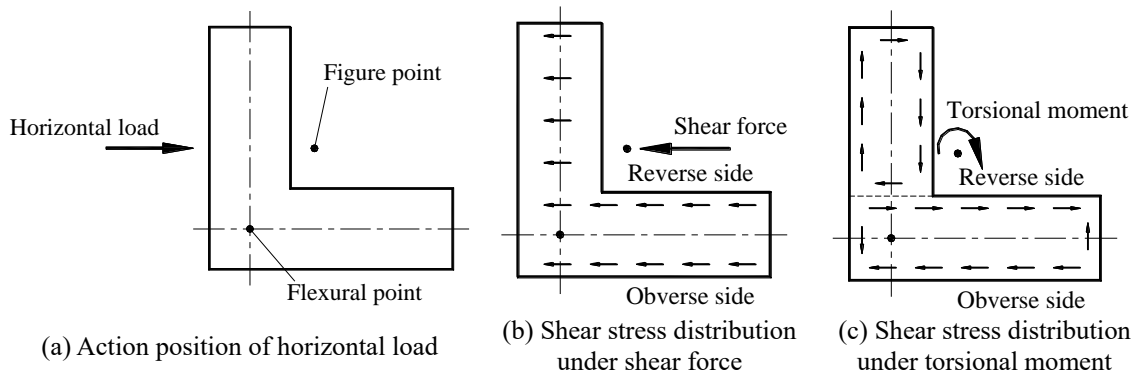


Fig. 11 Mechanical state of the joint core of corner joint

The shear stress of the section, generated by the shear force, is equal between the obverse side and the reverse side (Fig. 10). But for the corner joint, the action line of horizontal load passes the figure center of L-shaped section rather than the flexural center (Fig. 11), and there is not only shear force but also torsional moment at the joint core section. The shear stress of the section results from the shear force and the torsional moment collectively. At the obverse side, the direction of shear stress generated by the shear force and the torsional moment is the same, but at the reverse side, the direction is opposite (Fig. 11). Consequently, the shear stress of the section at the obverse side is greater than that at the reverse side.

### 3.2 Load-displacement curve

The load-displacement hysteretic curves of the specimens are shown in Fig. 12. It is showed that the hysteretic loops are plump, which are in shuttle or bow shape, indicating that SRC special-shaped column-beam joints have good hysteretic performance.

The load-displacement skeleton curves are shown in Fig. 13. Three critical characteristic points, namely, yield point, ultimate point and failure point can be obtained from the skeleton curves as shown in Fig. 14, and the loads and displacements corresponding to these three points are listed in Table 3. The yield point ( $P_y, \Delta_y$ ) can be determined using the graphical method (Nie *et al.* 2008a) (Fig. 14). The ultimate load  $P_u$  is selected as the maximum load, and the failure displacement  $\Delta_f$  is

defined as the maximum displacement corresponding to the load no less than  $0.85P_u$ . From Fig. 13 and Table 3, it can be found that TJ1 and TJ2 (or LJ1 and LJ2) have the approximate loading capacity, showing that with different steel forms, there is no significant impact on the loading capacity of SRC special-shaped column-beam joints, which are designed reasonably. In addition, the loading capacity of TJ3 (or LJ3), of which the ratio of column height to thickness is larger, is much higher than that of TJ1 (or LJ1).

### 3.3. Ductility

Ductility is one of the most significant indexes to evaluate the seismic performance of the structure. The displacement ductility coefficient  $\mu$  can be calculated as the ratio of failure displacement  $\Delta_f$  to the yield displacement  $\Delta_y$ . The displacement ductility coefficients of all specimens are listed in Table 3, indicating good ductility of SRC special-shaped column-beam joints. By comparing, observations can be made as follows:

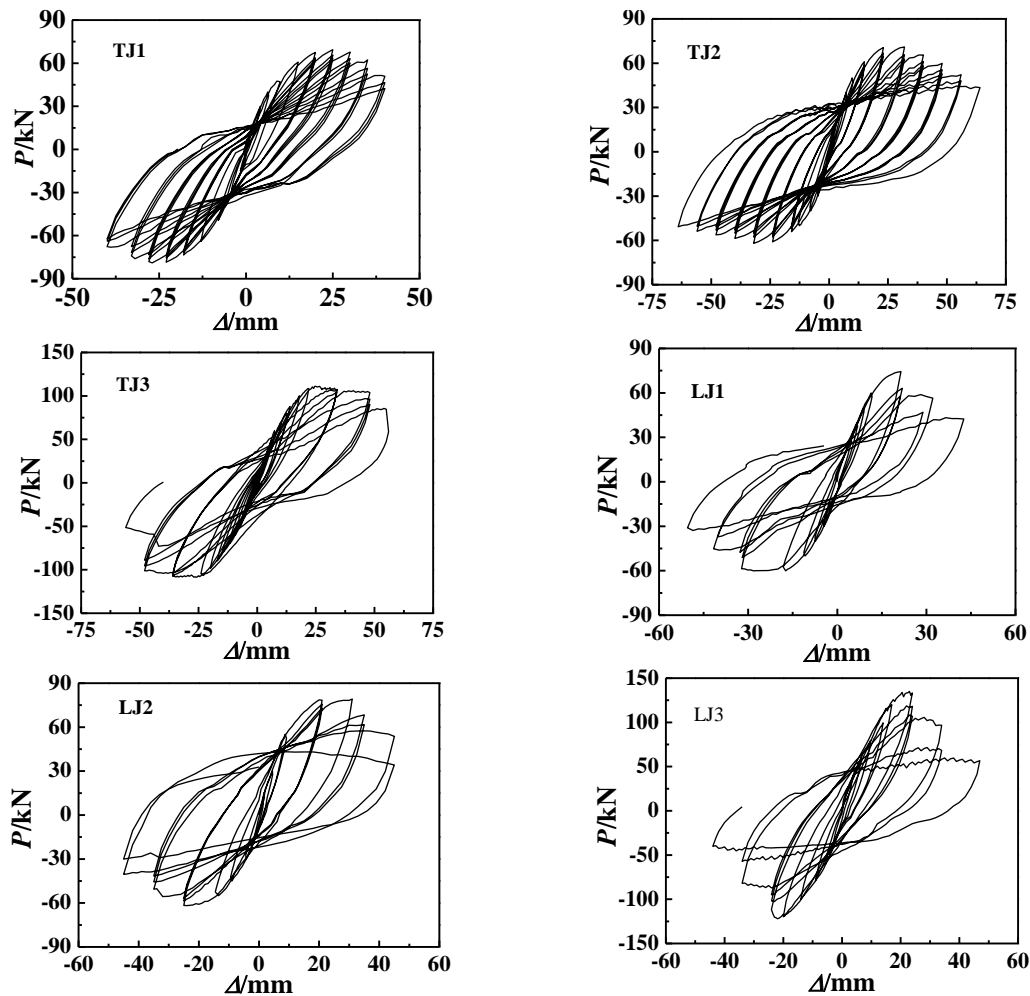


Fig. 12 Load-displacement hysteretic curves

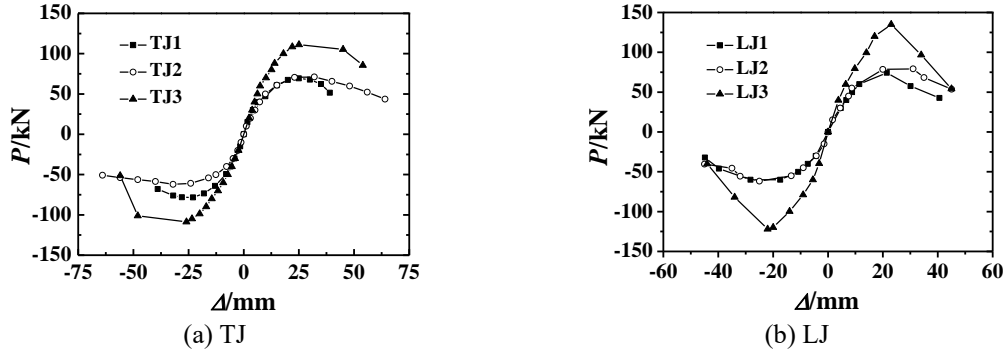


Fig. 13 Load-displacement skeleton curves

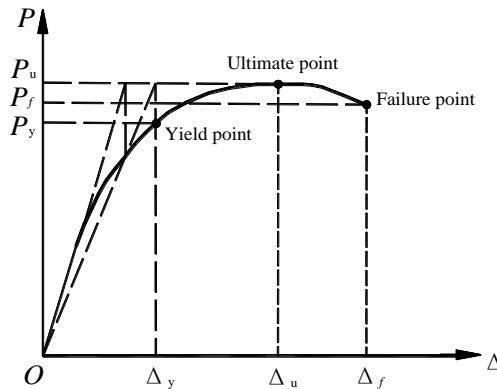


Fig. 14 Characteristic points on load-displacement curve

Table 3 Summary of measured results

Specimen	Loading direction	$P_y$ (kN)	$\Delta_y$ (mm)	$P_u$ (kN)	$\Delta_u$ (mm)	$P_f$ (kN)	$\Delta_f$ (mm)	$\mu = \Delta_f / \Delta_y$
TJ1	Positive	46.5	9.5	69.3	25.0	58.9	36.2	3.82
	Negative	58.5	11.1	78.4	23.0	68.0	39.0	3.51
TJ2	Positive	58.5	13.8	71.0	32.0	60.4	47.2	3.42
	Negative	50.0	12.6	62.0	32.0	52.7	59.0	4.68
TJ3	Positive	85.9	13.6	111.1	25.0	94.4	50.0	3.68
	Negative	82.2	15.0	108.8	26.0	92.5	49.4	3.29
LJ1	Positive	63.1	12.4	74.4	21.4	63.2	27.6	2.22
	Negative	47.0	9.7	60.1	28.2	51.1	37.2	3.84
LJ2	Positive	63.0	12.5	79.2	31.0	67.3	35.7	2.85
	Negative	45.1	9.1	61.7	25.0	52.4	33.0	3.67
LJ3	Positive	94.4	13.0	135.0	23.0	114.8	30.0	2.31
	Negative	84.0	10.2	122.0	22.0	103.7	29.4	2.88

The ductility of exterior joint (TJ) is much better than that of corner joint (LJ), as shown in Fig. 15(a). The reason is that the shear force and the torsional moment act collectively at the joint core

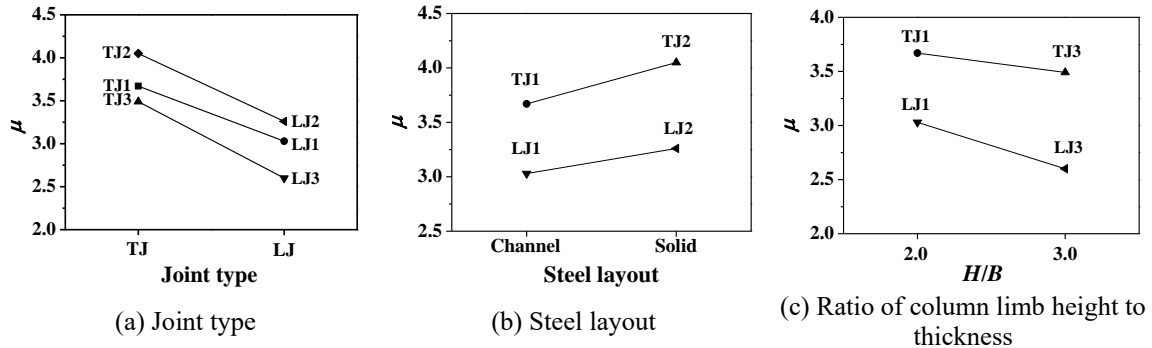


Fig. 15 Impact of different parameters on ductility

of corner joint, but only the shear force acts at the joint core of exterior joint. Consequently, the damage of specimens LJ was more serious than that of specimens TJ. The ductility of SRC special-shaped column-beam joints with solid web steel skeletons is better than that with channel steel trusses, as shown in Fig. 15(b). With the increasing of ratio of column limb height to thickness, the ductility of SRC special-shaped column-beam joints becomes worse, as shown in Fig. 15(c).

### 3.4 Stiffness degradations

Stiffness of the specimen under low cyclic reversed load can be expressed in the way of secant stiffness that is the ratio between the positive or negative maximum load and the corresponding displacement at every load cycle. As shown in Fig. 16, the stiffness of all specimens degrades evidently during the loading process, which is defined as stiffness degradation. The stiffness of the specimen TJ3 (or LJ3), of which the ratio of column limb height to thickness is 3, is much higher than that of the specimen TJ1 (or LJ1), of which the ratio of column limb height to thickness is 2. The stiffness between the specimens TJ1 (or LJ1) with channel steel truss and TJ2 (or LJ2) with solid web steel skeleton is roughly close to each other.

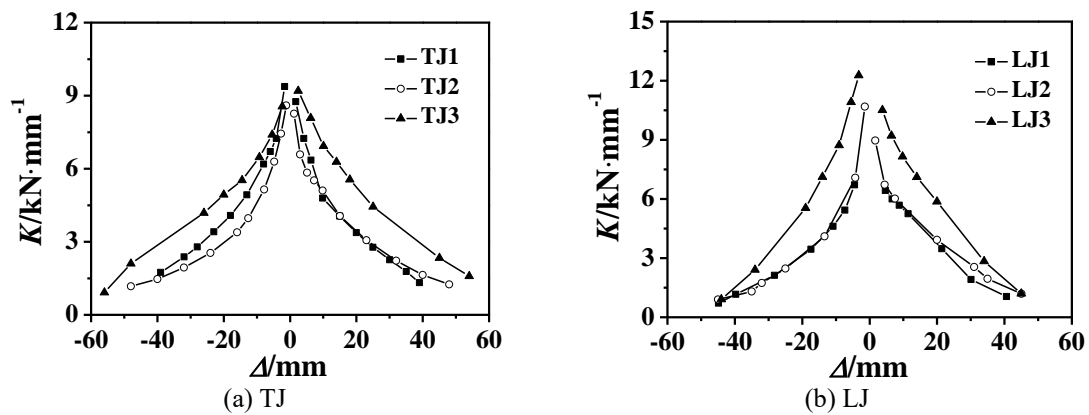


Fig. 16 Stiffness degradation

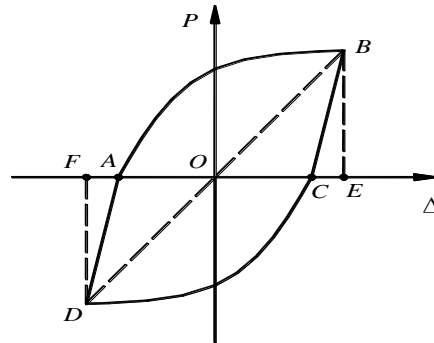


Fig. 17 Calculation of equivalent viscous damping coefficient

### 3.5 Energy dissipation capacity

Energy dissipation capacity is an important seismic performance index for the structure, which is usually represented by equivalent viscous damping coefficient  $h_e$  (Chou and Uang 2002b), and the formula for calculating  $h_e$  can be written as

$$h_e = \frac{1}{2\pi} \cdot \frac{S_{(ABCD)}}{S_{(OBE+ODF)}} \tag{1}$$

where  $S_{(ABCD)}$  and  $S_{(OBE+ODF)}$  represents the area of hysteretic loop ABCDA and triangles OBE and ODF respectively, which are showed in Fig. 17.

The  $h_e-\Delta/\Delta_y$  curves of all specimens are illustrated in Fig. 18. It can be seen that the energy dissipations are steadily and evidently enhanced with the increasing of displacement. Although  $h_e$  of the specimens TJ1 and TJ2 is close,  $h_e$  of the specimen LJ2 is higher than that of the specimen LJ1, showing that the energy dissipation capacity of SRC special-shaped column-beam joint with solid web steel skeleton is superior to that with channel steel truss. Compared with the specimen TJ1 (or LJ1),  $h_e$  of the specimen TJ3 (or LJ3) is lower in the early stage of loading, but higher in the later stage of loading, and the displacement indicated by the dividing point (Fig. 18) approximates  $2\Delta_y$ . In view of this, it can be found that the energy dissipation capacity of SRC special-shaped column-beam joints, under the circumstance of large deformation, becomes better as the increasing of ratio of column limb height to thickness.

### 3.6 Shear deformation of joint core

The shear deformation occurs at the joint core under the shear force. Fig. 19 shows the shear deformation of the joint core (Ciutina and Dubina 2008b). It can be seen that the joint core changes from rectangle to rhombus periodically under cyclic loads. Through measuring the changing diagonal length of the joint core, the relative rotation of the joint core, that is the shear deformation of the joint core, can be calculated as followed

$$\bar{X} = \frac{\delta_1 + \delta_1' + \delta_2 + \delta_2'}{2} \tag{2}$$

$$\sin \theta = \frac{b}{\sqrt{a^2 + b^2}}, \quad \cos \theta = \frac{a}{\sqrt{a^2 + b^2}} \quad (3)$$

$$\alpha_1 = \frac{\sin \theta \cdot \bar{X}}{a}, \quad \alpha_2 = \frac{\cos \theta \cdot \bar{X}}{b} \quad (4)$$

$$\gamma = \alpha_1 + \alpha_2 = \frac{\sin \theta \cdot \bar{X}}{a} + \frac{\cos \theta \cdot \bar{X}}{b} = \frac{\sqrt{a^2 + b^2}}{ab} \bar{X} \quad (5)$$

In which  $\gamma$  is the joint core rotation,  $(\delta_1 + \delta_1')$  and  $(\delta_2 + \delta_2')$  are the relative displacements (in absolute value) recorded by dial gauges,  $a$  and  $b$  are the vertical and horizontal dimensions between the measuring points.

Due to the crack and crush of concrete, the changing process of the shear deformation of the joint core has not been recorded. So the shear deformation of the joint core at the characteristic point is only illustrated in Fig.20. It can be seen that the relative rotation of the joint core at the failure point of all specimens is greater than 0.02rad, and the maximum rotation can even reach to 0.046rad, indicating the shear failure of the joint core again. The shear deformation of the joint core of SRC special-shaped column-beam joint with channel steel truss (the specimen TJ1 or LJ1)

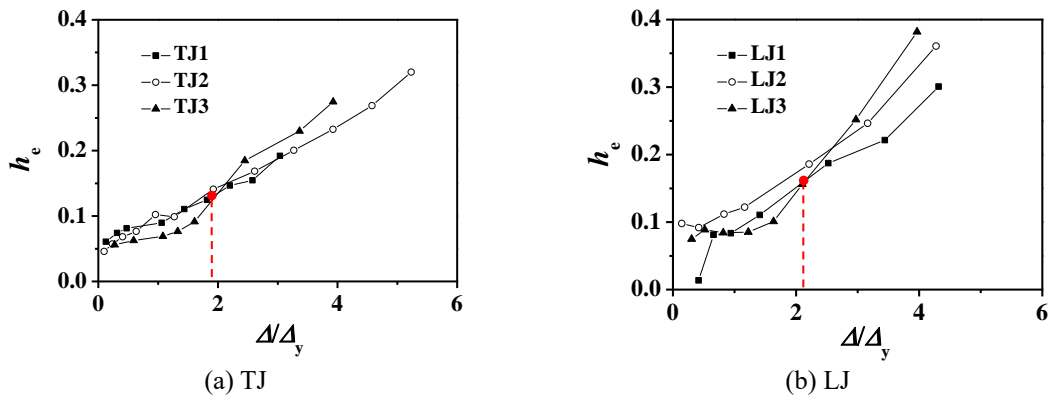


Fig. 18 Energy dissipation capacity

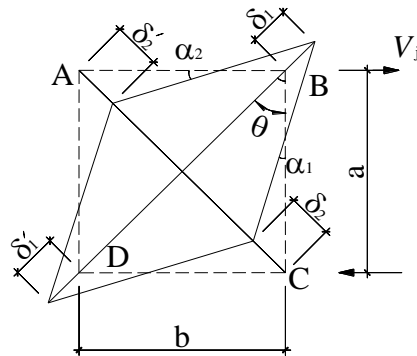


Fig. 19 Shear deformation of the joint core

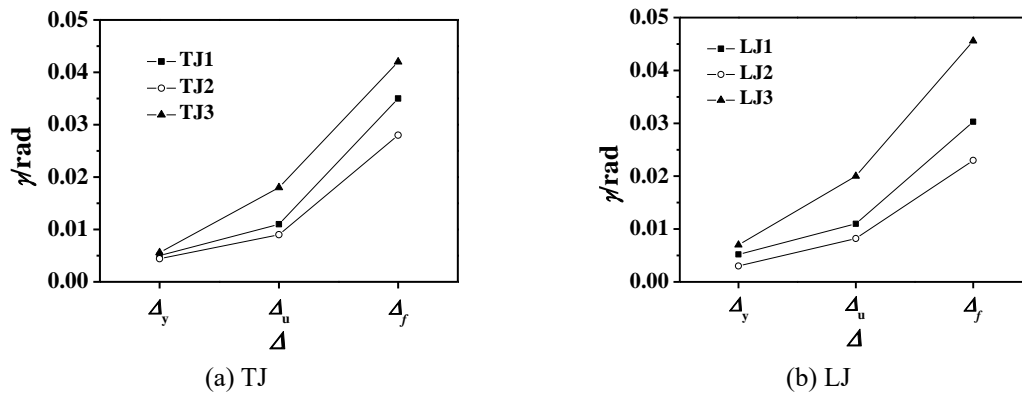


Fig. 20 Relative rotation of joint core at the characteristic points

is larger than that with solid web steel skeleton (the specimen TJ2 or LJ2). With the increasing of the ratio of column limb height to thickness, the shear deformation of the joint core becomes larger, as shown that the relative rotation of the joint core of the specimen TJ3 (or LJ3), of which the ratio of column limb height to thickness is 3, is larger than that of the specimen TJ1 (or LJ1), of which the ratio of column limb height to thickness is 2.

#### 4. Conclusions

The purpose of this investigation was to study the seismic behavior of SRC special-shaped column-beam joints. Based on the experimental results described in this paper, the following conclusions can be drawn:

- The failure mode of all specimens is the shear failure of the joint core, and the relative rotation of the joint core was greater than 0.02. The failure degree between the two sides of joint core is similar for the exterior joint (TJ), but different for the corner joints (LJ).
- The hysteretic loops of the specimens are plump, indicating good ductility and energy dissipation capacity.
- The joints with solid web steel skeleton illustrate better ductility and energy dissipation capacity than that with channel steel truss, but the loading capacity and stiffness of both are roughly close.
- With the increasing of the ratio of column limb height to thickness, the joints illustrate higher loading capacity and stiffness, better energy dissipation capacity, but worse ductility.

#### Acknowledgements

The authors would like to thank the financial support provided by Natural Science Foundation of China (Granted No.51308444), Natural Science Basic Research Foundation of Shaanxi Province (Granted No.2014JQ7288) and Program for Innovation Team of Education Ministry of China (Granted No.IRT13089), Shanxi Province (Granted No.2014KCT-31) and Xi'an University of Architecture and Technology.

## References

- Balaji, K.V.G.D. and Murty, D.S.R. (2001). "Reliability analysis of RC T-shaped column sections", *Indian Concrete J.*, **75**(3), 223-227.
- Cao, W.L., Hu, G.Z., Cui, L.C., Zhou, M.J., Hao, C.S. and Qu, Y.H. (2002a). "Experimental and analysis of seismic behavior of the +, L, T-shaped columns with concealed columns", *J. Build. Struct.*, **23**(1), 16-20. (in Chinese)
- Chen, C.C., Suswanto, B. and Lin, Y.J. (2009). "Behavior and strength of steel reinforced concrete beam-column joints with single-side force inputs", *J. Constr. Steel Res.*, **65**(8), 1569-1581.
- Chen, Z.P., Zhang, X.D., Su, Y.S. and Zhao, H.T. (2006). "A new type of concrete special-shaped columns-study of steel reinforced concrete special-shaped columns concept system", *Sichuan Build. Sci.*, **32**(2), 25-27. (in Chinese)
- Chou, C.C. and Uang, C.M. (2002b). "Cyclic performance of a type of steel beam to steel-encased reinforced concrete column moment connection", *J. Constr. Steel Res.*, **58**(5-8), 637-663.
- Ciutina, A.L. and Dubina, D. (2008b). "Column web stiffening of steel beam-to-column joints subjected to seismic actions", *J. Struct. Eng.*, ASCE, **134**(3), 505-510.
- Dundar, C. and Sahin, B. (1993). "Arbitrarily shaped reinforced concrete members subjected to biaxial bending and axial load", *Comput. Struct.*, **49**(4), 643-662.
- Ellobody, E. and Yong, B. (2011b). "Numerical simulation of concrete encased steel composite columns", *J. Constr. Steel Res.*, **67**(2), 211-222.
- Kim, C.S., Park, H.G. and Chung, K.S. (2012c), "Eccentric axial load testing for concrete-encased steel columns using 800MPa steel and 100MPa Concrete", *J. Struct. Eng.*, **138**(8), 1019-1031.
- Nie, J.G., Qin, K. and Cai, C.S. (2008a), "Seismic behavior of connections composed of CFSSTCs and steel-concrete composite beams: finite element analysis", *J. Constr. Steel Res.*, **64**(6), 680-688.
- Rong, X., Zhang, J.X. and Li, Y.Y. (2013), "Seismic behavior of specially shaped column joints with X-shaped reinforcement", *Transactions of Tianjin University*, **19**(2), 110-117.
- Sinha, S.N. (1996), "Design of cross (+) section of column", *Indian Concrete J.*, **70**(3), 153-158.
- Tokgoz, S. and Dundar, C. (2012d), "Test of eccentrically loaded L-shaped section steel fibre high strength reinforced concrete and composite columns", *Eng. Struct.*, **38**, 134-141.
- Tu, Y.Q., Shen, Y.F., Zeng, Y.G. and Ma, L.Y. (2014), "Hysteretic behavior of multi-cell T-shaped concrete-filled steel tubular columns", *Thin-Wall. Struct.*, **85**, 106-116.
- Xiao, J.Z., Li, J. and Chen, J. (2011a), "Experimental study on the seismic response of braced reinforced concrete frame with irregular columns", *Earthq. Eng. Eng. Vib.*, **10**(4), 487-494.
- Xue, J.Y., Chen, Z.P., Zhao, H.T., Gao, L. and Liu, Z.Q. (2012b), "Shear mechanism and bearing capacity calculation on steel reinforced concrete special-shaped columns", *Steel Compos. Struct.*, **13**(5), 473-487.
- Zhou, T., Chen, Z.H. and Liu, H.B. (2012a), "Seismic behavior of special shaped column composed of concrete filled steel tubes", *J. Constr. Steel Res.*, **75**, 131-141.